Simultaneous determination of dopamine, uric acid and estriol in maternal urine samples based on the synergetic effect of reduced graphene oxide, silver nanowires and silver nanoparticles in their ternary 3D nanocomposite

Qian Zhao[a], Yousef Faraj[abc]*, Lu-Yue Liu[a], Wei Wang[ab], Rui Xie[ab], Zhuang Liu[ab], Xiao-Jie Ju[ab], Jie Wei[a], Liang-Yin Chu[ab]

[a] *School of Chemical Engineering, Sichuan University, Chengdu 610065, Sichuan, P. R. China.*

[b] *State Key Laboratory of Polymer Materials Engineering, Sichuan University, Chengdu 610065, Sichuan, P. R. China.*

[c] *Department of Chemical Engineering, Faculty of Science and Engineering, University of Chester, Chester CH2 4NU, UK.*

*Corresponding author at: Department of Chemical Engineering, Faculty of Science and Engineering, University of Chester, Chester CH2 4NU, UK.

Telephone: 0044 (1484) 652247

E-mail address: y.faraj@chester.ac.uk

Abstract

A facile and efficient electrochemical biosensing platform based on screen printed carbon electrode (SPCE) modified with three-dimensional (3D) nanocomposite consists of reduced graphene oxide (RGO) with the insertion of silver nanowires (AgNWs) followed by the anchoring of silver nanoparticles (AgNPs) is constructed as RGO/AgNWs/AgNPs/SPCE for the simultaneous determination of dopamine (DA), uric acid (UA) and estriol (EST). The morphology characteristic and surface elemental composition of RGO/AgNWs/AgNPs nanocomposite are investigated by field-emission scanning electron microscope, transmission electron microscope and X-ray photoelectron spectroscope. Cyclic voltammetry, electrochemical impedance spectroscopy, linear sweep voltammetry and differential pulse voltammetry are utilized to explore the electrochemical performances of the constructed electrodes. Due to abundant active sites and excellent electrocatalytic activity of the nanocomposite, the RGO/AgNWs/AgNPs/SPCE sensor exhibits well-resolved oxidation peaks and enhanced oxidation peak currents in the ternary mixture of DA, UA and EST with respective linear response ranges of 0.6 to 50 μM, 1 to 100 μM and 1 to 90 μM and detection limits (S/N = 3) of 0.16 μM, 0.58 μM and 0.58 μM, respectively. Moreover, the constructed biosensor exhibits good selectivity, reproducibility and stability, and excellent performance in determining DA, UA and EST in synthetic urine samples with excellent recovery. The results reveal that the RGO/AgNWs/AgNPs nanocomposite is a promising candidate for advanced electrode material in electrochemical sensing field and possesses great application prospects in further sensing researches.

Keywords: simultaneous electrochemical determination; reduced graphene oxide; silver nanowire; dopamine; uric acid; estriol.

1. Introduction

Some biomolecules can affect maternal health and fetal development. Dopamine (DA), uric acid (UA) and estriol (EST) are some important examples of these biomolecules. DA, a crucial neurotransmitter belonging to the catecholamine family, plays a major role in controlling cognition, locomotion, emotion and memory [1]. When at abnormal concentration levels, DA can cause neurological disorders in pregnant women such as irritability [2], depression [3] and schizophrenia [4], and could potentially increase the risk for developing fetal growth restriction. UA, which is the primary end product of purine metabolism process, may lead to a number of diseases such as gout, diabetes, arthritis and hyperuricemia if its concentration is at an abnormal level in urine and serum [5]. Pregnant women may have high levels of UA because of high intakes of nutrients, including high purine foods, to meet the body's needs. EST, as the most abundant estrogen in pregnant women, is biosynthesized by the reactions between fetus and placenta [6, 7]. Thus, EST level, which can be determined from maternal blood or urine, can be used as a marker of fetal health and wellbeing. Therefore, the determination of these three biomolecules throughout women's pregnancy is of particular importance for maintaining pregnancy, the health of pregnant women and fetal viability.

In recent years, various methods have been employed to determine levels of DA, UA and EST, including high performance liquid chromatography [8, 9], spectrophotometric method [10], electrochemical method [11, 12], electrophoresis [13, 14] and so on. Among these methods, electrochemical method has been widely accepted as an ideal approach due to relatively low cost, simple operation, swift response and availability for in-situ monitoring [11, 15, 16]. However, the

coexistence of DA, UA and EST in the physiological fluids of pregnant women poses a great challenge to the electrochemical determination of these biomolecules using conventional electrodes. In addition, conventional electrodes possess relatively weak electrochemical catalytic activity, resulting in comparatively small signals response to these three biomolecules. To address these limitations, considerable efforts have been devoted to explore efficient electrode materials such as reduced graphene oxide/Sb_2O_5 [17], graphene decorated with gold nanoparticles [18], carbon nanotubes [19] and poly(3,4-ethylenedioxythiophene) doped with graphene oxide [20] for the improved determination of DA, UA and EST. Nevertheless, to the best of our knowledge, no electrode material has been reported for the simultaneous determination of these three biomolecules so far. Hence, seeking novel and efficient electrode materials is vital to rapidly, accurately and economically determine these biological compounds.

Reduced graphene oxide (RGO), a graphene derivate, has emerged as one of the most exciting material for chemical and biological sensing applications, due to its unparalled electrical conductivity, outstanding electronic and mechanic properties and large surface area and so on [21]. Nonetheless, some limitations of RGO such as surface defects inevitably introduced in the reduction of GO [22, 23] as well as the tendency of agglomeration in water [24, 25], resulting in loss of active sites and a decrease in electrical conductivity. Therefore, researchers have focused their attention upon functionalization and attachment of metallic nanomaterials on the surfaces of RGO nanosheets, using conducting polymers, metal–organic frameworks and organic crystals [26], in a bid to significantly tailor its physiochemical properties. Amongst all the materials, Ag nanomaterials have earned prodigious attention for the merits such as comparatively low cost, good electrocatalytic

activity, ultra-high electrical conductivity, low toxicity, fantastic biocompatibility and antibacterial activity [27, 28]. Silver nanoparticles (AgNPs) have been extensively explored and utilized in biological sensing platforms. The immobilization of AgNPs on RGO does not only fix the defects on the surface of RGO, but also hinder the agglomeration of AgNPs with a "flexible confinement" served by RGO [29]. In a recent study, the modification of glassy carbon electrode (GCE) with RGO/AgNPs was reported for the determination of EST from 0.1 to 3 μM with the detection limit of 21 nM [30]. Kaur *et al.* established the AgNPs/RGO based electrochemical biosensor, which exhibited favorable sensitivity and selectivity in the simultaneous determination of DA and UA [31]. Lately, silver nanowires (AgNWs) have become a rising star for the development of biosensors and electronics. The intercalation of AgNWs into RGO layers is highly beneficial for constructing electrical conductive pathways, restraining the restacking of RGO sheets and also preventing the agglomeration of AgNWs [29, 32]. Li *et al*. developed AgNW/RGO nanocomposites as electrode materials for the simultaneous determination of ascorbic acid (AA), DA and UA, achieving good separation of oxidation peaks and enhancement of peak currents [32]. The functionalization of RGO with AgNPs and AgNWs together should come as a big surprise in sensing and sensor-related fields, offering synergistic effects. It is worth mentioning that no report is available in literature, where AgNPs and AgNWs are used together in functionalization of RGO for the determination of biomolecules.

Screen printing technology is a well-established technique for the fabrication of screen printed electrodes (SPE), which have been widely used in the fields of environment, pharmaceutics, biomedicine and industry for the past few years [33]. With the features of

portability, good repeatability, low-cost mass production and microliter-level demands of samples, screen printed carbon electrode (SPCE) has been demonstrated as a prospective candidate electrode in on-site electrochemical sensing applications [33, 34]. On account of this, it is quite significant to exploit novel SPCEs for the on-site testing of biomolecules.

Therefore, in this study, a novel electrochemical biosensor is developed by integrating SPCE and RGO-based three-dimensional (3D) nanocomposite RGO/AgNWs/AgNPs (RGO/AgNWs/AgNPs/SPCE), which is designed with the insertion of AgNWs between RGO sheets followed by the anchoring of AgNPs on the surfaces of both RGO and AgNWs, as shown in Fig. 1, for the sensitive and simultaneous determination of DA, UA and EST in their ternary mixture. On account of numerous active sites and fascinating electrocatalytic activity provided by the nanocomposite, the RGO/AgNWs/AgNPs/SPCE could exhibit high selectivity and sensitivity. The as-fabricated biosensor is successfully applied to simultaneously determining the above-mentioned three biomolecules in synthetic urine.

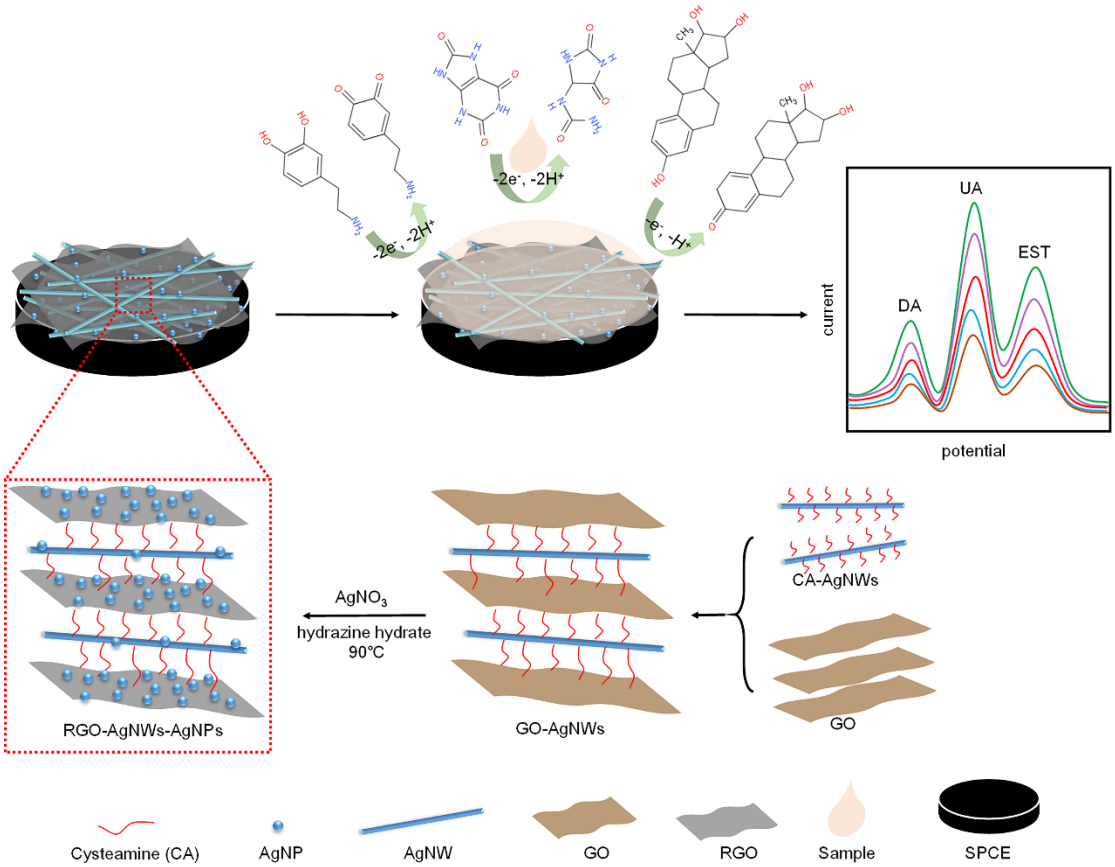

Fig. 1. Preparation process of RGO/AgNWs/AgNPs and electrochemical determination of DA, UA and EST using RGO/AgNWs/AgNPs/SPCE.

2. Material and methods

2.1 Materials

Dopamine (DA, H8502), uric acid (UA, ≥ 99%), ascorbic acid (AA, ≥ 99%), glucose (≥ 99.5%), urea (99-100.5%), progesterone (≥ 99%) and polyvinylpyrrolidone (PVP) (weight-average molecular weight, Mw = 55,000) were purchased from Sigma-Aldrich. Estriol (EST, analytical standard) and cysteamine (CA, 95%) were obtained from Aladdin. Graphene oxide (GO, XF002-3) was purchased from Nanjing XFNANO Materials Tech Co., Ltd. Silver nitrate ($AgNO_3$, 99%), ethylene glycol (EG), sodium chloride (NaCl), hydrazine hydrate (80%), potassium ferricyanide ($K_3[Fe(CN)_6]$), potassium ferrocyanide ($K_4[Fe(CN)_6]\cdot 3H_2O$) and potassium chloride (KCl) were all

purchased from Chengdu Kelong Chemical Reagents. A 0.01 M phosphate buffered solution (PBS) was prepared by PBS powder purchased from Beijing Solarbio Science & Technology Co., Ltd., adjusting the pH as required with phosphoric acid. Synthetic urine (CF-003) was purchased from Dongguan Changfeng Technology Co., Ltd. Other chemicals and solvents were of analytical grade and used as received without further purification. Deionized water (18.2 MΩ cm, 25 ℃) used throughout the experiments was supplied from Milli-Q Plus water purification system (Millipore).

2.2 Apparatus of material characterization and electrochemical measurements

Cyclic voltammetry (CV), linear sweep voltammetry (LSV) and differential pulse voltammetry (DPV) measurements were carried out using a potentiostat (PGSTAT 101, Metrohm) equipped with Nova 2.1 software. The electrochemical impedance spectroscopy (EIS) measurements were performed on an electrochemical analyzer (CHI 660E, Chenhua). The screen printed carbon electrodes (SPCEs) (DS150, Metrohm) utilized for electrochemical studies consist of a carbon (C) working electrode (W.E.), a platinum (Pt) counter electrode (C.E.) and a silver (Ag) reference electrode (R.E.) (Fig. S1). The surface morphology of materials was examined by means of Field-Emission Scanning Electron Microscope (FESEM) (JSM-7500F, JEOL) and Transmission Electron Microscope (TEM) (JEM-2100F, JEOL). The surface elemental composition was analyzed via X-ray Photoelectron Spectroscope (XPS) (XSAM800, Kratos) using MgKα as radiation source.

2.3 Preparation of AgNWs and GO/AgNWs

AgNWs were prepared by the modified polyol synthesis method [35]. In a typical experiment, 20 mL of PVP solution (1 M in EG) was mixed with 20 mL of $AgNO_3$ solution (0.2 M in EG) in a beaker, followed by the addition of 4.68 mg of NaCl. Then, the mixture was transferred into an autoclave and heated at 140 ℃ for 1 h. The precipitate was purified

by centrifugation and thoroughly washed with water and ethanol. The as-obtained AgNWs were dried and collected by vacuum freeze-drying technology.

GO/AgNWs were prepared according to a previously reported method [32]. Briefly, the mixture of AgNWs (80 mg) and cysteamine (240 mg) dispersed in ethanol (200 mL) was stirred for 16 h at room temperature. Then, the precipitate (CA-AgNWs) was collected by centrifugation and vacuum freeze-drying technology for the subsequent decoration of GO. In a typical preparation of GO/AgNWs, 5 mg of CA-AgNWs and 20 mg of GO were dispersed in 50 mL deionized water. The mixture was then placed into a water bath at 50 °C and stirred for 20 h to obtain GO/AgNWs.

2.4 Preparation of RGO/AgNWs/AgNPs

The preparation of RGO/AgNWs/AgNPs was carried out by using hydrazine hydrate as reducing agent [36]. The specific procedure modified from a previously reported method was designed as follows. 50 mL of the as-synthesized GO/AgNWs solution was mixed with 10 mL of $AgNO_3$ solution (5 mg/mL). The mixture was put in an oil bath and heated up to 90 °C under constant stirring, followed by the addition of 5 mL of hydrazine hydrate drop by drop and stirred further for 2 h at 90 °C. After cooling to room temperature, the resulting precipitate was centrifuged and washed with water for several times and dried by vacuum freeze-drying technology.

For the comparative study, RGO/AgNPs, RGO/AgNWs and RGO were also prepared by hydrazine hydrate using the above-mentioned procedure.

2.5 Fabrication of electrodes

1 mg of RGO/AgNWs/AgNPs was dispersed in 2 mL of solvent (a mixture of deionized water and ethanol with a volume ratio of 4:1) with ultrasonic mixing for 1 h. Before coating, the SPCEs

with a working area of 0.11 cm^2 were rinsed several times with deionized water and dried by a warm air system. Then, 8 μL of the above suspension was uniformly dropped onto the working area of the SPCEs and dried in air to fabricate RGO/AgNWs/AgNPs/SPCE. For the purpose of comparison, RGO/AgNPs/SPCE, RGO/AgNWs/SPCE and RGO/SPCE were fabricated in the same way.

2.6 Electrochemical measurements

CV and EIS measurements were performed in a solution containing 1 mM $[Fe(CN)_6]^{3-/4-}$ and 0.1 M KCl for the electrochemical characterizations of the bare and modified SPCEs. CV measurements were recorded at a scan rate of 50 mV s^{-1}. EIS measurement was recorded with a frequency range of 0.01 Hz to 100 kHz. DPV, LSV and CV measurements were performed for the electrochemical determination of DA, UA and EST. DPV measurements were performed with a step potential of 5 mV, modulation amplitude of 50 mV, modulation time of 0.05 s and scan rate of 25 mV s^{-1} were used.

3. Results and discussion

3.1 Material characterization

The surface morphological studies of AgNWs, CA-AgNWs, GO, GO/AgNWs and RGO/AgNWs/AgNPs are conducted by FESEM and TEM. As shown in Fig. 2(a), the as-synthesized AgNWs exhibit a uniform shape with a mean diameter ca. 75 nm, suggesting the successful preparation of AgNWs with the chemical reduction of $AgNO_3$ by EG. Cysteamine, as an additional functional group, is used to modify the AgNWs, through which the AgNWs are attached onto the surface of GO sheets. The surface morphology of CA-AgNWs is shown in Fig. 2(b). It can be seen that cysteamine molecules adsorbed on the surface of AgNWs, owing to the formation of the S-Ag covalent bond by the reaction

between the thiol (-SH) group of cysteamine and Ag atoms on the surface of AgNWs [37], suggesting the successful modification of AgNWs with cysteamine. Fig. 2(c) shows representative FESEM image of GO with a smooth surface. Fig. 2(d) shows the FESEM image of GO/AgNWs, in which it is apparent that AgNWs are attached onto the surface of GO through the exposed amine (-NH2) groups on CA-AgNWs reacting with the abundant epoxy functional groups on GO, demonstrating the formation of AgNWs on the surface of GO sheets. Figs. 2(e, f) represent the morphologies of RGO/AgNWs/AgNPs with different amplifications, in which AgNPs with a varying size (mean ca. 35 nm) are either dispersed onto RGO or around AgNWs, indicating successful synthesis of RGO/AgNWs/AgNPs using hydrazine hydrate as reductant. It is worth noting that the existence of AgNWs and AgNPs prevents the agglomeration of RGO because of the 3D morphological microstructure of RGO/AgNWs/AgNPs.

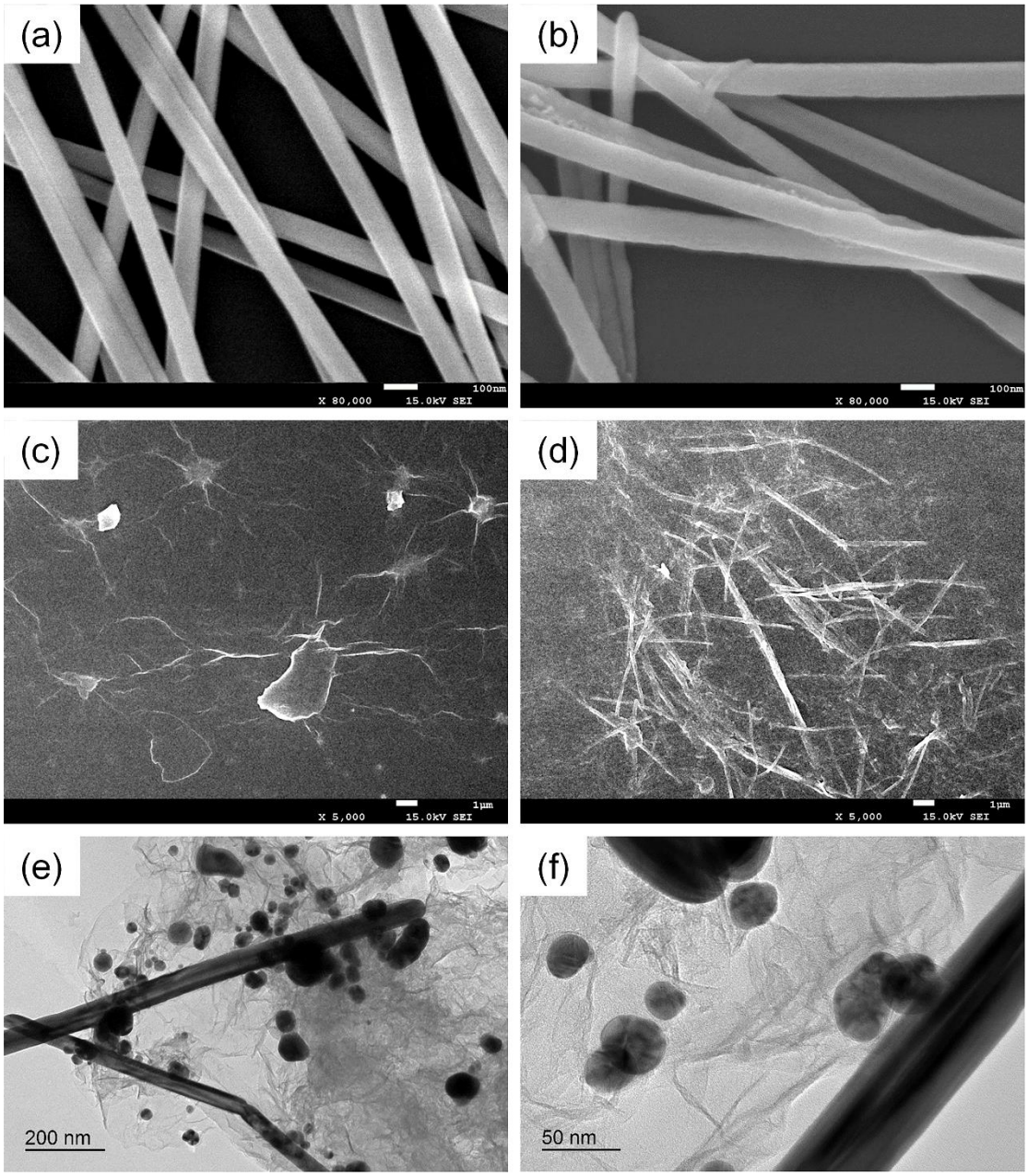

Fig. 2. (a-d) FESEM images of AgNWs (a), CA-AgNWs (b), GO (c) and GO/AgNWs (d). (e, f) TEM images of RGO/AgNWs/AgNPs with different magnifications. The scale bar is 100 nm, 100 nm, 1 μm, 1 μm, 200 nm and 50 nm in a, b, c, d, e and f, respectively.

The surface elemental compositions of GO, GO/AgNWs and RGO/AgNWs/AgNPs are determined using XPS analysis. The survey XPS spectrum of RGO/AgNWs/AgNPs shows the presence of O, N, Ag, C and S elements (Fig. S2(a)), revealing the successful synthesis of

RGO/AgNWs/AgNPs. Fig. S2(b) clearly shows the Ag $3d_{3/2}$ and $3d_{5/2}$ doublet of RGO/AgNWs/AgNPs. The binding energies of Ag $3d_{3/2}$ and Ag $3d_{5/2}$ peaks are 374.25 and 368.25 eV, respectively, which prove unambiguously that Ag in nanocomposite is present only in the metallic form [38], suggesting the successful introduction of AgNWs and AgNPs into RGO layers. The atomic concentration of GO, GO/AgNWs and RGO/AgNWs/AgNPs are shown in Table S1. It can be seen that the C/O atom ratio of GO/AgNWs is 2.26, slightly higher than that of GO, suggesting that there is only a low degree of reduction of GO in the formation of GO/AgNWs. While RGO/AgNWs/AgNPs have a C/O atom ratio of 8.59, far more than that of GO, indicating the successful preparation of RGO/AgNWs/AgNPs with a high degree of reduction by hydrazine hydrate.

3.2 Electrochemical characterization

The electrochemical performances of different SPCEs are recorded via CV in 0.1 M KCl solution containing 1 mM $[Fe(CN)_6]^{3-/4-}$ (Fig. S3(a)). A pair of well-defined redox peaks corresponding to $[Fe(CN)_6]^{3-/4-}$ are observed for all SPCEs. The bare SPCE shows the lowest peak current with the separation of peak potentials (ΔE_P) of 228 mV, suggesting the sluggish electron transfer at the surface of bare SPCE. After modification of the SPCE with RGO, an increase in the peak current and a decrease in the ΔE_P are observed, indicating that RGO can facilitate the rate of electron transfer. Compared with RGO/SPCE, RGO/AgNWs/SPCE and RGO/AgNPs/SPCE exhibit higher peak currents and lower ΔE_P values, which are attributed to the high electrocatalytic activity and conductivity of AgNWs and AgNPs. The highest peak current appears with the lowest ΔE_P of 132 mV at RGO/AgNWs/AgNPs/SPCE, revealing the fact that RGO/AgNWs/AgNPs enhance the rate

of electron transfer, which could be attributed to the superior electrocatalytic effect and unique synergistic structure of RGO/AgNWs/AgNPs.

The capabilities of bare and different modified SPCEs in terms of electron transfer are also investigated by EIS. The electron transfer resistance (R_{et}) is equal to the diameter of the high-frequency semicircle in the Nyquist curve, controlling the electron transfer kinetics of the redox probe at the surface of electrodes. The Nyquist curves are acquired in the solution of 1 mM $[Fe(CN)_6]^{3-/4-}$ and 0.1 M KCl (Fig. S3(b)). Bare SPCE exhibits the biggest semicircle with R_{et} of about 1320 Ω, indicating the poor capability of electron transfer. After the modification with RGO, the semicircle diameter of RGO/SPCE is significantly decreased, suggesting the presence of RGO on the SPCE facilitates fast electron transfer rate. In comparison with RGO/SPCE, a decrease in the semicircle diameter is appeared at RGO/AgNWs/SPCE with R_{et} of approximately 609 Ω, owing to the high electrocatalytic performance and conductivity of AgNWs. Similar result occurs with RGO/AgNPs/SPCE, which demonstrates a smaller semicircle than RGO/AgNWs/SPCE. It seems that RGO/AgNWs/AgNPs/SPCE shows a straight line without the high-frequency semicircle. However, a very small arc can be observed with RGO/AgNWs/AgNPs/SPCE, demonstrating the synergistic structure and excellent electrocatalytic activity of RGO/AgNWs/AgNPs that bring about a higher electron transfer rate.

3.3 Electrochemical oxidation behaviors of DA, UA, and EST

The electrochemical oxidation behaviors of DA, UA, and EST on bare and modified SPCEs are investigated in 0.01 M PBS (pH 3.5) with LSV. Figs. S4(a-c) show LSV curves of DA, UA and EST recorded individually at different SPCEs, respectively. It is obvious that the oxidation peak currents of the three biomolecules at RGO/AgNWs/AgNPs/SPCE are significantly increased when

compared to bare and the other modified SPCEs, indicating that RGO/AgNWs/AgNPs have a strong catalytic effect on the electrochemical oxidation of DA, UA and EST. Fig. S4(d) shows LSV curves obtained in the simultaneous measurements of DA, UA and EST at different SPCEs. Two poorly defined peaks are observed at bare SPCE, possibly resulting from the overlapping oxidation peaks of DA, UA and EST. While the oxidation peaks at the potentials of 0.35 V, 0.50 V and 0.71 V corresponding respectively to DA, UA and EST are clearly discernible at all modified SPCEs. In addition, the highest oxidation peak current of DA, UA and EST are obtained at RGO/AgNWs/AgNPs/SPCE. These results reveal the superior electrochemical catalytic property of RGO/AgNWs/AgNPs, which could be ascribed to 3D morphological microstructure and the synergistic effects of RGO, AgNWs and AgNPs.

3.4 Optimization of experimental parameters

The concentration of RGO/AgNWs/AgNPs is a significant factor in the electrochemical response of RGO/AgNWs/AgNPs/SPCE to DA, UA and EST. Therefore, RGO/AgNWs/AgNPs/SPCEs with different concentrations (0.1, 0.3, 0.5, 0.75 and 1 mg/mL) are analyzed by LSV respectively, as shown in Fig. S5(a). It is clearly seen that the oxidation peak currents of DA, UA and EST reach the maximum when the concentration of RGO/AgNWs/AgNPs is 0.5 mg/mL. The oxidation peak currents of these three biomolecules decrease gradually with both the high concentrations and the low concentrations of RGO/AgNWs/AgNPs. The former may result from obstructions of the electron transfer caused by the restacking of RGO/AgNWs/AgNPs and the latter could be resulted from the insufficient active sites. Based on the results, 0.5 mg/mL is selected as the optimum concentration for subsequent experiments.

The effects of the pH of PBS on the electrochemical behaviors of DA, UA and EST at RGO/AgNWs/AgNPs/SPCE are also studied by LSV in 0.01 M PBS with the pH range of 1.5-5.5 (Fig. S5(b, c)). Obviously in Fig. S5(b), the oxidation peak current of DA, UA and EST increases gradually with increasing pH and then decreases dramatically with further increase in pH. The oxidation peak current of DA and UA reaches the maximum at pH 3.5, while the maximum oxidation peak current of EST is obtained at pH 2.5. In Fig. S5(c), the oxidation peak potential of DA, UA and EST shifts towards more negative values with the increase of pH, which reveals that protons are involved in the redox reactions of the three biomolecules at the surface of RGO/AgNWs/AgNPs/SPCE. Moreover, the ΔE_P for DA, UA and EST at pH 3.5 is sufficient to obtain distinct oxidation peaks of these molecules. Therefore, with comprehensive consideration, pH 3.5 is chosen for the following electrochemical determinations of DA, UA and EST.

3.5 Effect of scan rate

The reaction kinetics of RGO/AgNWs/AgNPs/SPCE are investigated by CV with increasing scan rate from 10 to 500 mV s^{-1}. Figs. S6(a, c, e) exhibit the individual CV curves of DA, UA and EST at various scan rates. As the scan rate increases, the oxidation peak current of DA, UA and EST increases continuously with the oxidation peak potentials shifting positively. Moreover, the linear relationships for DA, UA and EST between the oxidation peak current and the square root of scan rate are established separately in Figs. S6(b, d, f), which reveal that the reaction kinetics for the oxidations of DA, UA and EST are dominated by diffusion controlled process, probably owing to the fast electron transfer rate on RGO/AgNWs/AgNPs/SPCE.

3.6 Determination of DA, UA and EST

The simultaneous determination of DA, UA and EST at RGO/AgNWs/AgNPs/SPCE is conducted by DPV in the ternary mixture, in which the concentration of one biomolecule is successively increased while those of the other two are kept constant. As illustrated in Figs. 3(a, c, e), the oxidation peaks of DA, UA and EST are found at 0.3 V, 0.45 V and 0.65 V, respectively. From Figs. 3(a, b), it can be seen that the oxidation peak current of DA linearly increases, whereas those of UA and EST remain almost unchanged with the increased DA concentration ranging 0.6-50 μM in the presence of 50 μM UA and 50 μM EST. Similar trends are depicted in the determination of UA with its concentration increasing from 1 to 100 μM in the solution containing 20 μM DA and 50 μM EST (Figs. 3(c, d)). Also , the oxidation peak current of EST shows an excellent linear relationship with its concentration ranging 1-90 μM in the presence of 10 μM DA and 10 μM UA (Figs. 3(e, f)). The limits of detection (LOD) for DA, UA and EST are respectively calculated as 0.16, 0.58 and 0.58 μM at three folds of the signal-to-noise ratio (S/N = 3). The comparison of the analytical performance of RGO/AgNWs/AgNPs/SPCE with those of the other modified electrodes reported in recent literatures for the determination of DA, UA and EST is summarized in Table 1. It is quite apparent that RGO/AgNWs/AgNPs modified SPCE developed in this work exhibits improved performance and achieves the first simultaneous determination of DA, UA and EST in their ternary mixture.

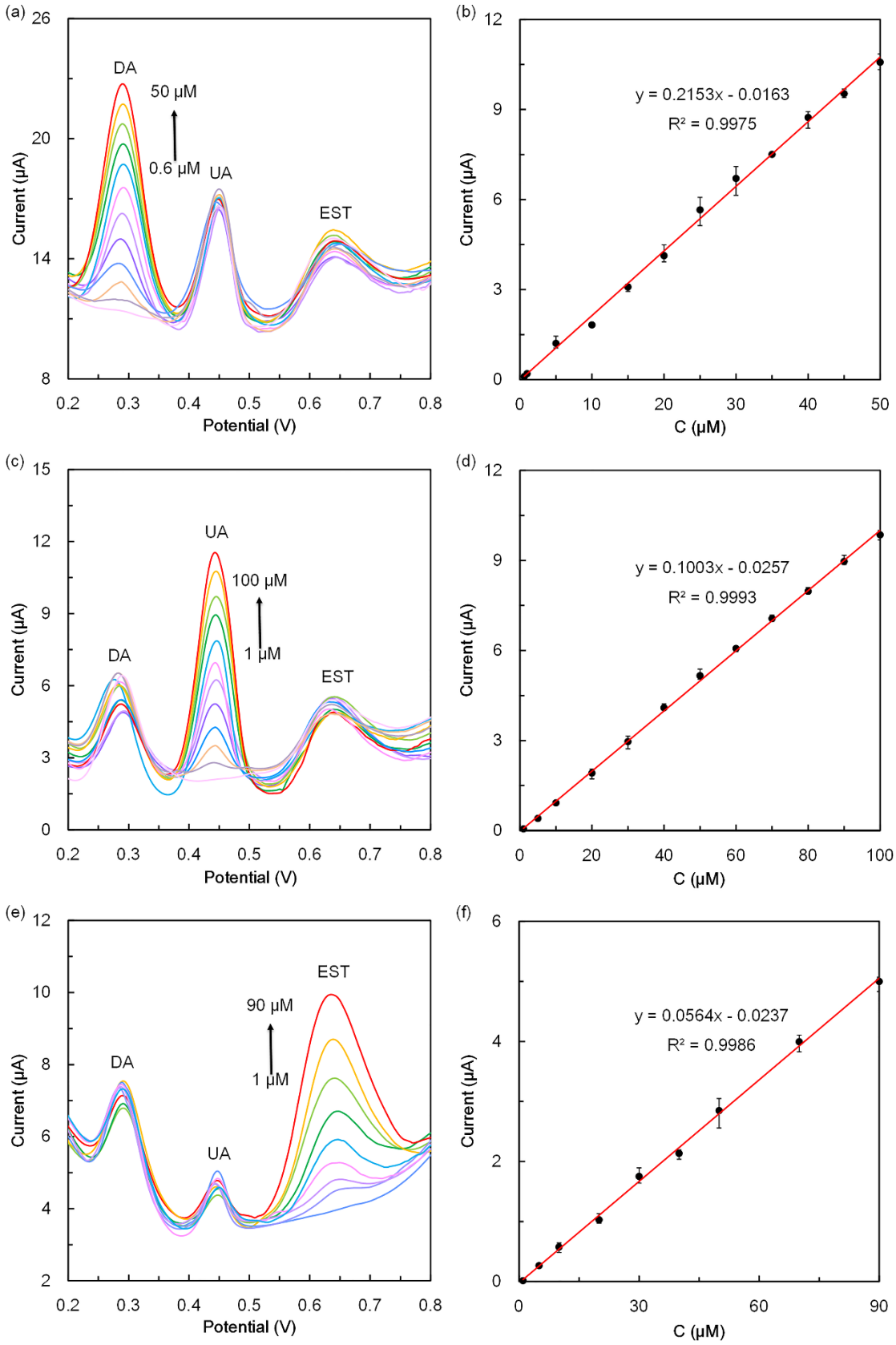

Fig. 3. (a, c, e) DPV curves of RGO/AgNWs/AgNPs/SPCE in 0.01 M PBS (pH 3.5) at DA concentrations of 0.6, 1, 5, 10, 15, 20, 25, 30, 35, 40, 45 and 50 μM in the presence of 50 μM UA

and 50 μM EST (a), UA concentrations of 1, 5, 10, 20, 30, 40, 50, 60, 70, 80, 90 and 100 μM in the presence of 20 μM DA and 50 μM EST (c), and EST concentrations of 1, 5, 10, 20, 30, 40, 50, 60, 70, 80 and 90 μM in the presence of 10 μM DA and 10 μM UA (e). (b, d, f) Plots of oxidation peak currents of DA (b), UA (d) and EST (f) versus sample concentrations.

Table 1 Comparison of RGO/AgNWs/AgNPs/SPCE with previously reported biosensors for the electrochemical determination of DA, UA and EST.

Electrode	Linear range (μM)			LOD (μM)			Ref.
	DA	UA	EST	DA	UA	EST	
RGO/AuNP/SPE	1-160	25-200	—	0.29	5.4	—	[18]
AgNW-rGO/SPCE	40-450	35-300	—	0.26	0.3	—	[32]
ND[a]/SPE	2-100	2-97	—	0.57	0.89	—	[39]
cs-SWCNT-IL[b]/SPCE	0.5-30	0.5-1000	—	0.16	0.17	—	[40]
Pt/MWCNTs/GCE	—	—	1-75	—	—	0.62	[12]
MWCNT/SPCE	—	—	1-1000	—	—	0.53	[19]
RGO-GNPs-PS[c]/GCE	—	—	1.5-22	—	—	0.48	[41]
Fe_3O_4 NPs/CPE[d]	—	—	3-111	—	—	2.75	[42]
RGO/AgNWs/AgNPs/SPCE	0.6-50	1-100	1-90	0.16	0.58	0.58	This work

[a] ND: nanodiamond. [b] cs-SWCNT-IL: chitosan solution-single walled carbon nanotubes-ionic liquid. [c] RGO-GNPs-PS: reduced graphene oxide-gold nanoparticles-and potato starch. [d] CPE: carbon paste electrode.

3.7 Interference, reproducibility and stability studies

Since a number of substances coexist in physiological fluids, the selectivity of the sensor composite material is an important property that has to be evaluated. In other words,

the measurement of the ability of the sensor to reject major interfering substances, such as glucose, urea, ascorbic acid and so on, is paramount. The interference study is carried out in 0.01 M PBS containing 15 μM DA, 20 μM UA, 40 μM EST and some interfering substances by DPV. Since the estrogen family consists of oestrone, estradiol and EST, the effects of oestrone and estradiol, along with other several substances, on the EST measurements are investigated in the interference study. However, it is worth mentioning that in a pregnant woman, EST is produced in a remarkable quantity with a 1000-fold increase, whereas the total levels of oestrone and estradiol increase by 100-fold [43]. This implies that the amount of EST is about 10 times higher than that of oestrone and estradiol combined in the urine of a pregnant women. Therefore, taking the above fact into consideration, the effects of 4 μM oestrone and 4 μM estradiol are investigated in this study. In addition, both oestrone and estradiol can be irreversibly converted into EST [43], which may render the effects of oestrone and estradiol somewhat negligible. It can be observed from Fig. 4 that the current signals corresponding to DA, UA and EST undergoes a very slight change (below 5%) in the presence of Na^+, Cl^-, ascorbic acid, glucose, urea, progesterone, oestrone and estradiol. The results suggest that the developed RGO/AgNWs/AgNPs/SPCE sensor shows excellent selectivity for the determination of DA, UA and EST, with no or very little disturbance from other substances, even if they coexist in the same solution.

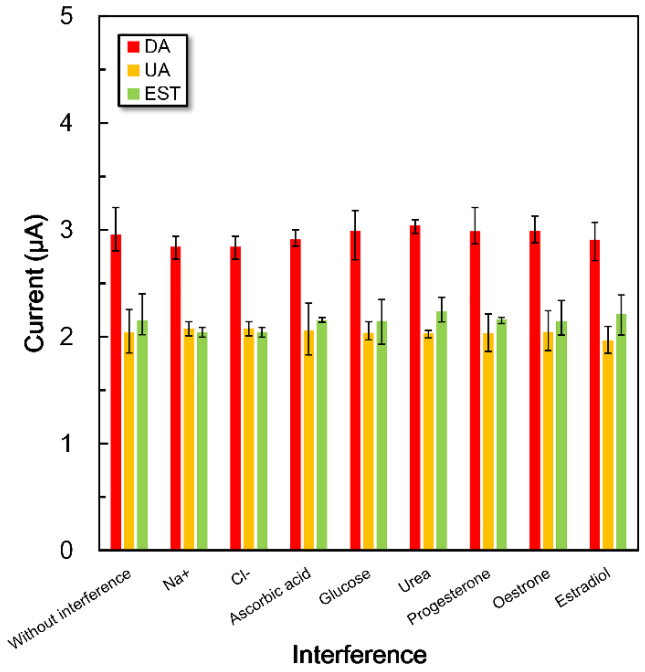

Fig. 4. Oxidation peak currents of 15 μM DA, 20 μM UA and 40 μM EST at RGO/AgNWs/AgNPs/SPCE by DPV in 0.01 M PBS (pH 3.5) before and after adding 3 mM Na^+, 3 mM Cl^-, 1 mM ascorbic acid, 2 mM glucose, 2 mM urea, 300 μM progesterone, 4 μM oestrone and 4 μM estradiol.

The reproducibility of RGO/AgNWs/AgNPs/SPCE sensor is evaluated by comparing five electrodes fabricated independently under the same condition. The relative standard deviation (RSD) of the oxidation peak currents is calculated to be as small as 3.93%, 2.16% and 2.41% for DA, UA and EST, respectively. The stability of RGO/AgNWs/AgNPs/SPCE sensor is tested using the electrode stored in the refrigerator for 15 days. The oxidation peak currents of DA, UA and EST are found to decay by only 7.59%, 6.48% and 8.56% respectively. These results clearly indicate that RGO/AgNWs/AgNPs/SPCE possesses a good reproducibility and stability.

3.8 Synthetic urine test

To illustrate the practicability of RGO/AgNWs/AgNPs/SPCE sensor, the as-fabricated sensor is used in the simultaneous determination of DA, UA and EST in synthetic urine, diluted 100 times

with 0.01 M PBS for measurements by the standard addition method, the analytical results of which are presented in Table 2. The recovery of RGO/AgNWs/AgNPs/SPCE ranges from 97.08% to 103.67% and the RSD (n = 5) is less than 5%, which provides a proof that RGO/AgNWs/AgNPs/SPCE can be effectively used for the simultaneous determination of DA, UA and EST in real urine samples.

Table 2 Performance of RGO/AgNWs/AgNPs/SPCE sensor in simultaneous determination of DA, UA and EST in synthetic urine samples (n = 5).

Sample	Analytes	Added (μM)	Found (μM)	Recovery (%)	RSD (%)
	DA	15	15.22	101.49	4.07
1	UA	15	15.55	103.67	3.81
	EST	20	19.42	97.08	4.42
	DA	15	14.79	98.60	4.03
2	UA	20	20.57	102.83	4.44
	EST	35	35.16	100.44	0.81
	DA	20	20.18	100.89	4.16
3	UA	20	20.18	100.88	4.65
	EST	30	29.82	99.39	3.60
	DA	20	20.10	100.52	4.67
4	UA	30	29.85	99.49	2.14
	EST	50	49.18	98.36	1.92

4. Conclusions

A 3D nanocomposite RGO/AgNWs/AgNPs has been successfully prepared and applied for the first time for the point-of-care simultaneous determination of DA, UA and EST. SPCE is integrated with the 3D nanocomposite RGO/AgNWs/AgNPs, which is designed with the insertion of AgNWs between RGO sheets followed by the anchoring of AgNPs on the surfaces of both RGO and AgNWs. The developed RGO/AgNWs/AgNPs/SPCE shows a significantly improved electron transfer kinetics for electroactive substances. The fabricated RGO/AgNWs/AgNPs/SPCE electrode exhibits superior electrocatalytic activity towards the oxidation of DA, UA and EST with significant increase in the peak currents. These excellent properties are attributed to unique structure and synergistic effects of RGO, AgNWs and AgNPs. Outstanding selectivity, good reproducibility and stability make RGO/AgNWs/AgNPs/SPCE effective for direct simultaneous determination of DA, UA and EST in real urine samples. Therefore, the developed sensor could provide a potential platform for the direct on-site analysis of DA, UA and EST in clinical diagnostics and bio-analytical applications. Furthermore, the RGO/AgNWs/AgNPs composite with special 3D microstructure and excellent performances is highly promising for electrochemical sensing and other electrocatalytic applications.

Declaration of interests

There are no conflicts to declare.

Acknowledgements

This work was supported by the National Natural Science Foundation of China [21490582]; Sichuan University Talent Introduction Fund and Innovative Research Team in University [201810611720, 201810610441]; and the State Key Laboratory of Polymer Materials Engineering [sklpme2018-2-01].

References

[1] X. Zhang, X. Chen, S. Kai, H.Y. Wang, J. Yang, F.G. Wu, Z. Chen, Highly sensitive and selective detection of dopamine using one-pot synthesized highly photoluminescent silicon nanoparticles, Anal Chem, 87 (2015) 3360-3365. https://doi.org/10.1021/ac504520g.

[2] X. Hui, X. Xuan, J. Kim, J.Y. Park, A highly flexible and selective dopamine sensor based on Pt-Au nanoparticle-modified laser-induced graphene, Electrochimica Acta, 328 (2019) 135066. https://doi.org/10.1016/j.electacta.2019.135066.

[3] P. Belujon, A.A. Grace, Dopamine system dysregulation in major depressive disorders, Int J Neuropsychopharmacol, 20 (2017) 1036-1046. https://doi.org/10.1093/ijnp/pyx056.

[4] H. Prata-Ribeiro, A. Ponte, G. Luisa, Dopamine, glutamate and biotypes in the future of schizophrenia, European Psychiatry, 41 (2017) S829-S829. https://doi.org/10.1016/j.eurpsy.2017.01.1625.

[5] W. Zhang, L. Liu, Y. Li, D. Wang, H. Ma, H. Ren, Y. Shi, Y. Han, B.C. Ye, Electrochemical sensing platform based on the biomass-derived microporous carbons for simultaneous determination of ascorbic acid, dopamine, and uric acid, Biosens Bioelectron, 121 (2018) 96-103. https://doi.org/10.1016/j.bios.2018.08.043.

[6] K.D. Santos, O.C. Braga, I.C. Vieira, A. Spinelli, Electroanalytical determination of estriol hormone using a boron-doped diamond electrode, Talanta, 80 (2010) 1999-2006. https://doi.org/10.1016/j.talanta.2009.10.058.

[7] E.S. Gomes, F.R.F. Leite, B.R.L. Ferraz, H. Mourao, A.R. Malagutti, Voltammetric sensor based on cobalt-poly(methionine)-modified glassy carbon electrode for determination of estriol hormone in pharmaceuticals and urine, J Pharm Anal, 9 (2019) 347-357. https://doi.org/10.1016/j.jpha.2019.04.001.

[8] B. Ferry, E.P. Gifu, I. Sandu, L. Denoroy, S. Parrot, Analysis of microdialysate monoamines,

including noradrenaline, dopamine and serotonin, using capillary ultra-high performance liquid chromatography and electrochemical detection, J Chromatogr B Analyt Technol Biomed Life Sci, 951-952 (2014) 52-57. https://doi.org/10.1016/j.jchromb.2014.01.023.

[9] S. Studzinska, B. Buszewski, Fast method for the resolution and determination of sex steroids in urine, J Chromatogr B Analyt Technol Biomed Life Sci, 927 (2013) 158-163. https://doi.org/10.1016/j.jchromb.2012.12.037.

[10] M.R. Moghadam, S. Dadfarnia, A.M. Shabani, P. Shahbazikhah, Chemometric-assisted kinetic-spectrophotometric method for simultaneous determination of ascorbic acid, uric acid, and dopamine, Anal Biochem, 410 (2011) 289-295. https://doi.org/10.1016/j.ab.2010.11.007.

[11] Z.H. Sheng, X.Q. Zheng, J.Y. Xu, W.J. Bao, F.B. Wang, X.H. Xia, Electrochemical sensor based on nitrogen doped graphene: simultaneous determination of ascorbic acid, dopamine and uric acid, Biosens Bioelectron, 34 (2012) 125-131. https://doi.org/10.1016/j.bios.2012.01.030.

[12] X. Lin, Y. Li, A sensitive determination of estrogens with a Pt nano-clusters/multi-walled carbon nanotubes modified glassy carbon electrode, Biosens Bioelectron, 22 (2006) 253-259. https://doi.org/10.1016/j.bios.2006.01.005.

[13] M. Zhao, M.F. Zhou, H. Feng, X.X. Cong, X.L. Wang, Determination of tryptophan, glutathione, and uric acid in human whole blood extract by capillary electrophoresis with a one-step electrochemically reduced graphene oxide modified microelectrode, Chromatographia, 79 (2016) 911-918. https://doi.org/10.1007/s10337-016-3115-z.

[14] S. Flor, S. Lucangioli, M. Contin, V. Tripodi, Simultaneous determination of nine endogenous steroids in human urine by polymeric-mixed micelle capillary electrophoresis, Electrophoresis, 31 (2010) 3305-3313. https://doi.org/10.1002/elps.201000096.

[15] M.Y. Emran, M.A. Shenashen, H. Morita, S.A. El-Safty, One-step selective screening of bioactive molecules in living cells using sulfur-doped microporous carbon, Biosensors and Bioelectronics, 109 (2018) 237-245. https://doi.org/10.1016/j.bios.2018.03.026.

[16] C.S. Lee, S.H. Yu, T.H. Kim, One-step electrochemical fabrication of reduced graphene oxide/gold nanoparticles nanocomposite-modified electrode for simultaneous detection of dopamine, ascorbic acid, and uric acid, Nanomaterials, 8 (2017) 17. https://doi.org/10.3390/nano8010017.

[17] F.H. Cincotto, T.C. Canevari, S.A.S. Machado, A. Sánchez, M.A.R. Barrio, R. Villalonga, J.M. Pingarrón, Reduced graphene oxide-Sb_2O_5 hybrid nanomaterial for the design of a laccase-based amperometric biosensor for estriol, Electrochimica Acta, 174 (2015) 332-339. https://doi.org/10.1016/j.electacta.2015.06.013.

[18] D. Ji, Z. Liu, L. Liu, S.S. Low, Y. Lu, X. Yu, L. Zhu, C. Li, Q. Liu, Smartphone-based integrated voltammetry system for simultaneous detection of ascorbic acid, dopamine, and uric acid with graphene and gold nanoparticles modified screen-printed electrodes, Biosens Bioelectron, 119 (2018) 55-62. https://doi.org/10.1016/j.bios.2018.07.074.

[19] L.M. Ochiai, D. Agustini, L.C.S. Figueiredo-Filho, C.E. Banks, L.H. Marcolino-Junior, M.F. Bergamini, Electroanalytical thread-device for estriol determination using screen-printed carbon electrodes modified with carbon nanotubes, Sensors and Actuators B: Chemical, 241 (2017) 978-984. https://doi.org/10.1016/j.snb.2016.10.150.

[20] D. Li, M. Liu, Y. Zhan, Q. Su, Y. Zhang, D. Zhang, Electrodeposited poly(3,4-ethylenedioxythiophene) doped with graphene oxide for the simultaneous voltammetric determination of ascorbic acid, dopamine and uric acid, Mikrochim Acta, 187 (2020) 94. https://doi.org/10.1007/s00604-019-4083-4.

[21] N.O. Weiss, H. Zhou, L. Liao, Y. Liu, S. Jiang, Y. Huang, X. Duan, Graphene: an emerging electronic material, Adv Mater, 24 (2012) 5782-5825. https://doi.org/10.1002/adma.201201482.

[22] K. Naito, N. Yoshinaga, E. Tsutsumi, Y. Akasaka, Transparent conducting film composed of graphene and silver nanowire stacked layers, Synthetic Metals, 175 (2013) 42-46. https://doi.org/10.1016/j.synthmet.2013.04.025.

[23] M.S. Lee, K. Lee, S.Y. Kim, H. Lee, J. Park, K.H. Choi, H.K. Kim, D.G. Kim, D.Y. Lee, S. Nam, J.U. Park, High-performance, transparent, and stretchable electrodes using graphene-metal nanowire hybrid structures, Nano Lett, 13 (2013) 2814-2821. https://doi.org/10.1021/nl401070p.

[24] R. Zacharia, H. Ulbricht, T. Hertel, Interlayer cohesive energy of graphite from thermal desorption of polyaromatic hydrocarbons, Physical Review B, 69 (2004) 155406. https://doi.org/10.1103/PhysRevB.69.155406.

[25] Z.-S. Wu, D.-W. Wang, W. Ren, J. Zhao, G. Zhou, F. Li, H.-M. Cheng, Anchoring hydrous RuO_2 on graphene sheets for high-performance electrochemical capacitors, Advanced Functional Materials, 20 (2010) 3595-3602. https://doi.org/10.1002/adfm.201001054.

[26] X. Huang, X. Qi, F. Boey, H. Zhang, Graphene-based composites, Chem Soc Rev, 41 (2012) 666-686. https://doi.org/10.1039/c1cs15078b.

[27] N. Saha, S. Dutta Gupta, Low-dose toxicity of biogenic silver nanoparticles fabricated by swertia chirata on root tips and flower buds of allium cepa, J Hazard Mater, 330 (2017) 18-28. https://doi.org/10.1016/j.jhazmat.2017.01.021.

[28] Y. He, S. Su, T. Xu, Y. Zhong, J.A. Zapien, J. Li, C. Fan, S.-T. Lee, Silicon nanowires-based highly-efficient SERS-active platform for ultrasensitive DNA detection, Nano Today, 6 (2011) 122-130. https://doi.org/10.1016/j.nantod.2011.02.004.

[29] G. Zhou, D.-W. Wang, F. Li, L. Zhang, N. Li, Z.-S. Wu, L. Wen, G.Q. Lu, H.-M. Cheng, Graphene-wrapped Fe_3O_4 anode material with improved reversible capacity and cyclic stability for lithium ion batteries, Chemistry of Materials, 22 (2010) 5306-5313. https://doi.org/10.1021/cm101532x.

[30] C.A. Donini, M.K.L. da Silva, R.P. Simões, I. Cesarino, Reduced graphene oxide modified with silver nanoparticles for the electrochemical detection of estriol, Journal of Electroanalytical Chemistry, 809 (2018) 67-73. https://doi.org/10.1016/j.jelechem.2017.12.054.

[31] B. Kaur, T. Pandiyan, B. Satpati, R. Srivastava, Simultaneous and sensitive determination of ascorbic acid, dopamine, uric acid, and tryptophan with silver nanoparticles-decorated reduced graphene oxide modified electrode, Colloids Surf B Biointerfaces, 111 (2013) 97-106. https://doi.org/10.1016/j.colsurfb.2013.05.023.

[32] S.-M. Li, Y.-S. Wang, S.-T. Hsiao, W.-H. Liao, C.-W. Lin, S.-Y. Yang, H.-W. Tien, C.-C.M. Ma, C.-C. Hu, Fabrication of a silver nanowire-reduced graphene oxide-based electrochemical biosensor and its enhanced sensitivity in the simultaneous determination of ascorbic acid, dopamine, and uric acid, Journal of Materials Chemistry C, 3 (2015) 9444-9453. https://doi.org/10.1039/C5TC01564B.

[33] A.S. Rajpurohit, A.K. Srivastava, Simultaneous electrochemical sensing of three prevalent anti-allergic drugs utilizing nanostructured manganese hexacyanoferrate/chitosan modified screen printed electrode, Sensors and Actuators B: Chemical, 294 (2019) 231-244. https://doi.org/10.1016/j.snb.2019.05.046.

[34] Y. Zhang, X. Jiang, J. Zhang, H. Zhang, Y. Li, Simultaneous voltammetric determination of acetaminophen and isoniazid using MXene modified screen-printed electrode, Biosens Bioelectron, 130 (2019) 315-321. https://doi.org/10.1016/j.bios.2019.01.043.

[35] Z. Yi, X. Xu, X. Tan, L. Liu, W. Zhang, Y. Yi, J. Luo, W. Yao, Y. Yi, T. Duan, Y. Tang, Microwave-

assisted polyol method rapid synthesis of high quality and yield Ag nanowires, Surface and Coatings Technology, 327 (2017) 118-125. https://doi.org/10.1016/j.surfcoat.2017.08.024.

[36] H. Zhang, X. Wang, Y. Li, C. Guo, C. Zhang, Preparation and characterization of silver-doped graphene-reinforced silver matrix bulk composite as a novel electrical contact material, Applied Physics A, 125 (2019) 86. https://doi.org/10.1007/s00339-019-2379-1.

[37] H.-W. Tien, S.-T. Hsiao, W.-H. Liao, Y.-H. Yu, F.-C. Lin, Y.-S. Wang, S.-M. Li, C.-C.M. Ma, Using self-assembly to prepare a graphene-silver nanowire hybrid film that is transparent and electrically conductive, Carbon, 58 (2013) 198-207. https://doi.org/10.1016/j.carbon.2013.02.051.

[38] J. Ma, J. Zhang, Z. Xiong, Y. Yong, X.S. Zhao, Preparation, characterization and antibacterial properties of silver-modified graphene oxide, J. Mater. Chem., 21 (2011) 3350-3352. https://doi.org/10.1039/C0JM02806A.

[39] M. Baccarin, S.J. Rowley-Neale, E.T.G. Cavalheiro, G.C. Smith, C.E. Banks, Nanodiamond based surface modified screen-printed electrodes for the simultaneous voltammetric determination of dopamine and uric acid, Mikrochim Acta, 186 (2019) 200. https://doi.org/10.1007/s00604-019-3315-y.

[40] E. Nagles, O. García-Beltrán, J.A. Calderón, Evaluation of the usefulness of a novel electrochemical sensor in detecting uric acid and dopamine in the presence of ascorbic acid using a screen-printed carbon electrode modified with single walled carbon nanotubes and ionic liquids, Electrochimica Acta, 258 (2017) 512-523. https://doi.org/10.1016/j.electacta.2017.11.093.

[41] L.V. Jodar, F.A. Santos, V. Zucolotto, B.C. Janegitz, Electrochemical sensor for estriol hormone detection in biological and environmental samples, Journal of Solid State Electrochemistry, 22 (2017) 1431-1438. https://doi.org/10.1007/s10008-017-3726-9.

[42] J.P. da Silveira, J.V. Piovesan, A. Spinelli, Carbon paste electrode modified with ferrimagnetic

nanoparticles for voltammetric detection of the hormone estriol, Microchemical Journal, 133 (2017) 22-30. https://doi.org/10.1016/j.microc.2017.03.010.

[43] R. Lappano, C. Rosano, P. De Marco, E.M. De Francesco, V. Pezzi, M. Maggiolini, Estriol acts as a GPR30 antagonist in estrogen receptor-negative breast cancer cells, Mol Cell Endocrinol, 320 (2010) 162-170. https://doi.org/10.1016/j.mce.2010.02.006.

- Novel 3D nanocomposite RGO/AgNWs/AgNPs was synthesized for electrochemical sensing.
- Nanocomposite is integrated with SPCE for simultaneous detection of DA, UA and EST.
- Synergistic effect exists among RGO, AgNWs and AgNPs.
- The sensor exhibits superior electrocatalytic activity and outstanding selectivity.
- Effective determination of Dopamine, Uric Acid and Estriol in urine samples.